Science
AAAS

Supplementary Materials for

# VDAC oligomers form mitochondrial pores that release small mtDNA fragments and promote lupus-like disease

Jeonghan Kim[1], Rajeev Gupta[2], Luz P. Blanco[3], Shutong Yang[1], Anna Shteinfer-Kuzmine[2], Kening Wang[4], Jun Zhu[5], Hee Eun Yoon[1], Xinghao Wang[3], Kerkhofs Martijn[6], Hyeog Kang[1], Alexandra L. Brown[1], Sung-Jun Park[1], Xihui Xu[1], Eddy Zandee van Rilland[1#], Myung K. Kim[1], Jeffrey I. Cohen[4], Mariana J. Kaplan[3], Varda Shoshan-Barmatz[2] and Jay H. Chung[1]*

Corresponding author. Email: chungj@nhlbi.nih.gov

**This PDF file includes:**

22 **Materials and Methods**

23 Cell culture and cellular component measurement

24 *Vdac1/3*$^{-/-}$ MEFs and *Bax/Bak*$^{-/-}$ MEFs with the respective WT littermate MEFs were
25 obtained from Dr. Jeffery D. Molkentin (University of Cincinnati). WT, *Vdac1*$^{-/-}$ and *Vdac3*$^{-/-}$
26 MEFs were obtained from Dr. B. Geert (KU Leuven). WT and *Cgas*$^{-/-}$ MEFs were obtained from
27 Dr. H. W. Virgin (Washington University School of Medicine). WT and *Irf3/Irf7*$^{-/-}$ MEFs were
28 obtained from Dr. H. Lazear (The University of North Carolina at Chapel Hill). WT and *Micu1*$^{-/-}$
29 MEFs were obtained from Dr. T. Finkel (NIH/NHLBI). All MEFs were grown in complete
30 Dulbecco's modified Eagle's medium (DMEM, Corning) supplemented with 10% fetal bovine
31 serum (FBS, Sigma-Aldrich) and 1% penicillin and streptomycin antibiotics, (Gibco) at 37°C with
32 5% $CO_2$. WT ($\rho^0$) and *Endog*$^{-/-}$ ($\rho^0$) MEFs were generated by incubation with ethidium bromide
33 (Invitrogen) in complete DMEM supplemented with 15% FBS, antibiotics, uridine (50 µg/ml),
34 and pyruvate (1 mM) for 5 months.

35 To generate MEFs with knockdown genes, MISSION shRNA Lentiviral Transduction
36 Particles (Sigma-Aldrich) against mouse *Endog* (SHCLNV-NM_007931) were purchased from
37 Sigma-Aldrich and MEFs were transduced with the shRNA encoding lentivirus stocks in the
38 presence of polybrene (8 µg/ml). Mouse *Cgas* (ON-TARGETplus *Mb21d1* siRNA: 214763), *Sting*
39 (ON-TARGETplus *Tmem173* siRNA: 72512), *Tbk1* (ON-TARGETplus *Tbk1* siRNA: 56480), and
40 control siRNA (ON-TARGETplus Non-targeting siRNA) were purchased from Dharmacon. The
41 siRNA transfection of MEFs was performed with 50 nM siRNA and Lipofectamine RNAiMAX
42 reagent (Invitrogen) according to the manufacturer's instructions. The expression vector for ΔN-
43 VDAC1 was generated by PCR using the primers shown in Table. S1A. The expression vector for
44 3A VDAC1 was generated by the QuikChange Site-Directed Mutagenesis Kit (Stratagene) with
45 the appropriate primers (Table. S1A). After transiently transfecting the expression vectors for WT,

46 ΔN- and 3A VDAC1 into *Vdac1/3*$^{-/-}$ MEFs, the ISG expression levels were measured and
47 normalized to overexpressed *Vdac1* mRNA levels.

48 Cellular cGAMP levels were measured by LC/MS (Agilent Technologies) using 5%
49 perchloric acid extracts of WT and *Endog*$^{-/-}$ MEFs. Intracellular ROS production in MEFs was
50 measured using the oxidative stress indicator CM-$H_2$DCFDA (Invitrogen) with flow cytometry
51 (BD Biosciences). The results of flow cytometry were analyzed using BD FACSDiva™ Software
52 (BD Biosciences). Mitochondrial ROS in MEFs were evaluated using the mitochondrial
53 superoxide indicator MitoSOX (Invitrogen) with a confocal microscope (LSM880, Zeiss)
54 equipped with a 63×/1.4 Plan-Apochromat lens (Zeiss). The confocal images were processed using
55 ZEN Imaging Software (Zeiss). To quantify mitochondrial ROS in human PBMCs, the cells were
56 obtained from heparinized blood using a Ficoll-Paque gradient. The cells were washed with
57 phosphate-buffered saline (PBS), resuspended in RPMI 1640 medium, and transferred to 96-well
58 plates. Subsequently, the cells were stimulated with the calcium ionophore A23187 (2.5 μM),
59 VBIT-4 (5 μM), and MitoSOX (10 μM) (Life Technologies) for 1 h. To determine the number of
60 cells per well, PicoGreen dye (100 pg/ml) was added to duplicate wells and the fluorescence
61 (Em/Ex 480/520) was measured at initiation of the experiment. After 30 min at 37°C, the
62 fluorescence was measured at 510/595 nm using a microplate reader (Synergy HTX; BIOTEK).
63 Cells without dye were used as the blank control. To perform cell type analysis of mitochondrial
64 ROS by VBIT-4, isolated PBMCs were stained for $CD14^{lo}$ (#325610, Biolegend), $CD15^{hi}$
65 (#301920, Biolegend) low-density granulocytes (LDG); $CD14^{hi}$, $CD15^{lo}$ Monocyte; $CD3^{+}$
66 (#300317, Biolegend), $CD19^{-}$ (#302232, Biolegend) T cell; $CD3^{-}$, $CD19^{+}$ B cell; $CD3^{-}$, $CD56^{+}$
67 (#362504, Biolegend) natural killer cell (NK cell). Cells were washed with PBS twice and pre-
68 treated with VBIT-4 (5 μM) for 10 min before A23187 (2.5 μM) and then incubated with MitoSOX

69 (10 μM) for 30 min. Cells were washed with PBS and resuspended cells were analyzed using flow
70 cytometry (Fortessa).
71
72 RNA sequencing and bioinformatic analyses
73 Total cellular RNA was extracted from WT and *Endog*$^{-/-}$ MEFs using the RNeasy Plus RNA
74 extraction kit (QIAGEN) and RNA integrity was verified by an Agilent Bioanalyzer. RNA
75 sequencing was performed in the NIH DNA Sequencing and Genomics core. RNA integrity was
76 first verified by an Agilent Bioanalyzer. Starting from 500 ng of total RNA, the TruSeq stranded
77 total RNA library preparation kit (Illumina) was used to construct RNAseq libraries following the
78 manufacturer's instructions. The resulting libraries were quantified by QuBit fluorometer (Thermo
79 Fisher) and sequenced on a Hiseq-3000 using a 2×50 bp modality. Data analysis of RNA
80 sequencing results was performed in the NIH-Bioinformatics and Computational Biology Core
81 Facility. Rigorous quality controls of paired-end reads were assessed using FastQC tools. Gene
82 expression levels were estimated for the GENCODE GTF reference database. Cohort gene
83 expression data was then assessed for outliers and irregular characteristics by reviewing properties
84 of summary distributions by unsupervised principle component analysis (PCA) using R and
85 manual review of the outcome. Differential expression analysis at the gene-level was carried out
86 using limma open source R/Bioconductor packages. The lmFit function in limma was used to Fit
87 linear models for each gene to calculate log2-fold changes and p-values using the normalized
88 factors as weights in the model. To account for multiple testing, the false discovery rate (FDR) via
89 the Benjamani–Hochberg algorithm was calculated. FDR q-values were estimated to correct the
90 p-values for the multiple testing issue.
91
92 RNA extraction and reverse-transcription quantitative PCR (RT-qPCR)

93 Total RNA was extracted using the RNeasy Plus Mini Kit (Qiagen) according to the
94 manufacturer's instructions. The first-strand cDNA was synthesized from 2 μg purified mRNA
95 using Accupower RT PreMix (BioNeer). The reaction mixtures were incubated at 42°C for 60 min
96 and 94°C for 5 min. RT-qPCR was performed using the LightCycler 96 system (Roche Life
97 Science) with SYBR Green master mix (Roche) and related primers (Table. S1B). GAPDH was
98 used as an internal standard of mRNA expression, and the ratio of the target gene expression to
99 GAPDH expression was calculated using LightCycler 96 Instrument software (Roche). The quality
100 of RT-qPCR results was evaluated based on the melting temperature ($T_m$) of a DNA fragment and
101 melting curve analysis.
102
103 Cell lysate preparation and immunoblot analysis
104 MEFs were harvested and washed twice with ice-cold PBS, and the pellets were lysed on ice
105 for 30 min in RIPA buffer. (50 mM Tris-HCl pH 7.4, 0.15 M NaCl, 1 mM EDTA, 1% NP-40, and
106 0.25% sodium deoxycholate) freshly supplemented with PhosSTOP phosphatase inhibitors
107 (Roche) and cOmplete™ protease inhibitors (Roche). Nuclear extracts were obtained using the
108 NE-PER Nuclear and Cytoplasmic Kit (Pierce) according to the manufacturer's instructions. The
109 total protein concentration was determined by Coomassie Plus protein assay (Thermo Fisher) and
110 subjected to immunoblotting. The following primary antibodies were used (1:1,000 dilution).
111 VDAC1 (ab14734, abcam); VDAC2 (#9412, Cell Signaling); VDAC3 (55060, Protein tech);
112 ENDOG (ab76122, abcam); IRF3 (#4302, Cell Signaling); phospho-IRF3 (#79945, Cell
113 Signaling); phospho-TBK1 (#5483, Cell Signaling); p-STAT1 (#9167, Cell Signaling); lamin B1
114 (#13435, Cell Signaling); ISG15 (#2743, Cell Signaling); IFI44 (MBS2528890, MyBioSource);
115 BAK (#12105, Cell signaling); BAX (#2772, Cell signaling); Caspase 3 (#14220, Cell signaling);
116 V5-Tag (#13202, Cell signaling); α-tubulin (sc-8035, Santa Cruz).

117

118 Quantification of mtDNA release

119 MEFs ($2\times10^6$ cells) were resuspended in 170 µl of digitonin buffer containing 150 mM NaCl,
120 50 mM HEPES pH 7.4, and 25 µg/ml digitonin (EMD Millipore Corp). The homogenates were
121 incubated on a rotator for 10 min at room temperature, followed by centrifugation at 16,000×*g* for
122 25 min at 4°C. A 1:20 dilution of the supernatant (cmtDNA) was used for qPCR. The pellet was
123 resuspended in 340 µl of lysis buffer containing 5 mM EDTA and proteinase K (Qiagen) and
124 incubated at 55°C overnight. The digested pellet was diluted with water (1:20 to 1:100) and heated
125 at 95°C for 20 min to inactivate proteinase K, and the sample was used for qPCR with mtDNA
126 specific primers (Table. S1C). The cmtDNA in the supernatant was normalized to the total mtDNA
127 in the pellet for each sample. For the quantification of fimtDNA release, MEFs were resuspended
128 in mitochondrial isolation buffer and subsequently homogenized 30 times with pestle B (small
129 clearance). The homogenized samples were centrifuged at 1,000×*g* for 10 min at 4°C. The
130 supernatant was transferred to a new tube and centrifuged at 1,000×*g* for 5 min at 4°C, and the
131 mitochondrial pellet was collected after the centrifugation of the final supernatant at 11,500×*g* for
132 10 min at 4°C. Isolated mitochondria were resuspended in 50 µl of CSK buffer containing 10 mM
133 PIPES pH 6.8, 300 mM sucrose, 100 mM NaCl, 3 mM $MgCl_2$, 1 mM EGTA, and 0.05% Triton
134 X-100 for 5 min on ice. The supernatant (fimtDNA) and CSK-pellet fractions were collected after
135 centrifugation at 17,000×*g* for 30 min at 4°C. A 1:20 dilution of CSK-sup was used for qPCR with
136 D-loop primers (Table. S1C). CSK-pellets were resuspended in 100 µl lysis buffer containing 5
137 mM EDTA and proteinase K and incubated at 56°C overnight. The digested pellet was diluted
138 with water (1:20 to 1:100) and heated at 95°C for 20 min, and the CSK-pellet fraction was used
139 for qPCR in each reaction. The fimtDNA in CSK-sup was normalized to the mtDNA in the CSK-
140 pellet.

141

142 Mitoplast isolation

143 Mitoplasts were isolated from the mitochondria of mouse liver. The liver tissue was washed
144 twice with ice-cold PBS and minced in mitochondrial isolation buffer containing 225 mM
145 mannitol, 75 mM sucrose, 5 mM MOPS, 0.5 mM EGTA, and 2 mM taurine (pH 7.25) with a
146 cOmplete™ protease inhibitor cocktail (Roche). The cells were ruptured by 10 Dounce
147 homogenizer strokes using pestle A (large clearance) for the initial strokes, followed by pestle B
148 using a pre-chilled Dounce homogenizer (abcam) for 25 strokes. The homogenized samples were
149 centrifuged at 1,000×*g* for 10 min at 4°C. The supernatant was transferred to a new tube, and the
150 mitochondrial pellet was collected after the centrifugation of the final supernatant at 11,500×*g* for
151 10 min at 4°C. Mitochondria were incubated in 20 mM $KH_2PO_4$ buffer for 40 min in a cold room.
152 After gentle agitation with a pipette, the samples were centrifuged at 4°C for 10 min at 8,000×*g*.
153 The 100 μg of mitoplasts were resuspended in mitoplast swelling buffer containing 125 mM
154 sucrose, 50 mM KCl, 5 mM HEPES, 2 mM $KH_2PO_4$, and 1 mM $MgCl_2$ (pH 7.2). The swelling
155 reactions were energized with 20 mM succinate to support swelling using 0.1 mM $H_2O_2$, 600 μM
156 $Fe^{2+}$, and 250 μM $Ca^{2+}$ for 10 min at 28°C with or without pre-incubation with 1.6 μM CsA. In
157 addition, 2 mM EDTA was added to prevent DNA degradation in the samples. After
158 centrifugation, the mtDNA in the supernatant was purified using QIAamp DNA Micro Kit
159 (Qiagen), and the mtDNA was detected using mouse mtDNA-specific primers.

160

161 Sequencing of fimtDNA and cmtDNA

162 To prepare the fimtDNA for sequencing, we isolated pure mitochondria from MEFs without
163 contamination from other organelles using the percoll gradient method (*1*). The fimtDNA was
164 prepared by incubating the pure mitochondria in the CSK buffer for 5 min on ice, and cmtDNA

165 was prepared by incubating the MEFs in the digitonin buffer for 10 min. Purified fimtDNA and
166 cmtDNA were used to construct NextGen sequencing libraries with ThruPLEX Plasma-seq Kit
167 (Takara) following the manufacturer's instructions. Sequencing data were acquired using the
168 Illumina MiSeq platform with a 2×75 bp modality. Raw sequence reads were first mapped to the
169 GRCm38 mouse reference genome excluding the mitochondrial genome reference by Burrows-
170 Wheeler Aligner (BWA) software (version 0.7.17) with default settings. In addition, the unmapped
171 reads were saved and aligned to the GRCm38 mitochondrial genome by BWA with default
172 settings. The SAMtools software (version 1.6) provided statistical information on the coverage of
173 mtDNA and the insert size of the paired mapped reads. The insert size distribution was computed
174 and plotted by the Kernel density estimation function in the R-stat package.
175
176 HSV-1 infection in MEFs
177 HSV-1 encoding mRFP fused to the N-terminus of VP26 (HSV-1-RFP; clone HSV F-GS
178 2822) was obtained from Dr. G.A. Smith at Northwestern University. The virus was titrated in
179 both Vero cells and WT MEFs. HSV-1-RFP was added and incubated at 37°C with 5% $CO_2$ for
180 1–2 days until isolated plaques were formed. The red fluorescence intensity was determined using
181 a UV fluorescence microscope (Olympus IX51) and flow cytometry (BD bioscience). To
182 determine the HSV-1-RFP growth curve, *Vdac1/3*$^{-/-}$ MEFs with the respective WT counterparts
183 were seeded in 12-well plates 1 d before infection and infected with HSV-1-RFP. Two aliquots of
184 the input virus were stored as 0 h samples, and infected cell plates were incubated at 37°C with
185 5% $CO_2$ for 1 h. The inoculum was removed from the 12-well plates, and the plates were further
186 cultured with fresh medium. At 3, 9, and 24 h post-infection, the infected MEFs were scraped in
187 their culture supernatant and subjected to 3 cycles of freeze and thaw, followed by centrifugation

188 to remove cell debris. The cell-free virus in the supernatant was stored at −80°C in a freezer and
189 subsequently titrated in Vero cells by plaque assay (*2*).
190
191 mtDNA–VDAC1 binding assay
192 For the mtDNA–peptide binding assay, the C-terminal biotinylated peptide corresponding to
193 a.a. residues 1–26 of mouse VDAC1 (MAVPPTYADLGKSARDVFTKGYGFGL) and the 3A
194 mutant peptide (MAVPPTYADLGASAADVFTAGYGFGL) were synthesized with acetylation
195 (N-terminus) and amidation (C-terminus) and purified by Genscript (Piscataway, NJ, USA).
196 Mitochondrial DNA was amplified using PCR with a mtDNA specific primer from the D-loop
197 region (Table. S1D). Purified mtDNA (120 bp) was incubated by rotating end-over-end with
198 peptides and Streptavidin Dynabeads (Invitrogen) for 18 h at 4°C. The peptides were captured by
199 the Streptavidin Dynabeads, and unbound peptides and free mtDNA were removed by extensive
200 washing with PBS. The samples were treated with proteinase K for 30 min at 60°C, and the
201 mtDNA in the supernatant was purified with QIAquick Nucleotide Removal Kit (Qiagen) and
202 quantified using qPCR with the D-loop3 primers (Table. S1C). Interaction of VDAC1–mtDNA in
203 the WT and *Endog*$^{-/-}$ MEFs was detected using an Immunoprecipitation Assay Kit (Millipore)
204 following the manufacturer's instructions with anti-VDAC1 antibody (ab14734, abcam) or normal-
205 mouse IgG (sc-2025, Santa Cruz) for negative control.
206
207 Mitochondrial and VDAC1 purification, channel reconstitution, recording and analysis
208 VDAC1 protein was purified from rat liver mitochondria using the celite:hydroxyapatite
209 column followed by carboxy methy cellulose chromatography method as previously described
210 (*3*). For conductance studies comparing WT and N-terminally (1–26 a.a.) truncated VDAC1 (ΔN-
211 VDAC1), we purified WT and ΔN-VDAC1 from *VDAC1*-deficient 293 HEK cells (by

212 CRISPR/Cas9 knockout method) transiently expressing the respective VDAC1. We transfected
213 pcDNA4/TO plasmid (0.5 μg DNA) encoding for full-length murine *Vdac1* or (ΔN-*Vdac1*) using
214 calcium phosphate. 48 h post-transfection, cells were harvested and VDAC1 and ΔN-VDAC1 were
215 purified as described for liver mitochondria (*3*)

216 Purified murine WT VDAC1 or ΔN-VDAC1 was reconstituted into a planar lipid bilayer
217 (PLB). Subsequently, single and multiple channel current recordings and data analysis were
218 carried out as previously described (*4*). Briefly, the PLB was prepared from soybean asolectin
219 dissolved in n-decane (30 mg/ml). Purified VDAC1 was added to the chamber defined as the cis
220 side containing 1 M NaCl, 10 mM HEPES, pH 7.4. Currents were recorded before and 15 min
221 after the addition of 37 nM mtDNA (47 bp) in the cis or trans compartment, under voltage-clamp
222 using a Bilayer Clamp BC-535B amplifier (Warner Instrument, Hamden, CT). The currents,
223 measured with respect to the trans side of the membrane (ground), were low-pass-filtered at 1 kHz
224 and digitized online using a Digidata1440-interface board and pClampex 10.2 software (Axon
225 Instruments, Union City, CA).

226

227 Micro-scale thermophoresis analysis

228 Microscale thermophoresis (MST) analysis was performed using a NanoTemper Monolith
229 NT.115 apparatus, as previously described (*5*). VDAC1 (162 nM) purified from rat liver was
230 fluorescently labeled using NanoTemper fluorescent protein-labeling Kit BLUE (L001,
231 NanoTemper Technologies, GmbH). A constant concentration of labeled VDAC1 was incubated
232 with increasing concentrations of mtDNA (3.9–196 nM) or VBIT-4 (0.625–100 μM) in buffer.
233 After 20 min of incubation, 3–5 μl of the samples were loaded into MST-grade glass capillaries
234 (Monolith NT Capillaries), and the thermophoresis process was performed (LED 20%, IR laser

235 80%) using the Monolith-NT115 apparatus. The results are presented as the bound fraction
236 calculated as follows: fraction bound 100 × ($F-F$ min)/($F$ max$-F$ min).
237
238 mtDNA efflux from liposomes reconstituted with VDAC1
239 Liposomes were prepared by the extrusion method using a mini-extruder purchased from
240 Avanti Polar Lipids Inc. (Alabaster, AL). Briefly, a thin lipid film was obtained by dissolving
241 soybean asolectin (10 mg/ml of chloroform) and then evaporating chloroform slowly under a
242 gentle stream of nitrogen gas. Next, the lipid film was hydrated in a buffer (10 mM Tricine, 150
243 mM NaCl, pH 7.4) containing 100 nM of mtDNA (47 bp) for 30–60 min at room temperature with
244 five vortex cycles (1 min separated by 1 min of rest). Then, mtDNA was added to the suspension
245 of large multilamellar vesicles, exposed to five freeze–thaw cycles using liquid nitrogen and
246 passed 11 times through the mini-extruder containing a polycarbonate filter (Whatman) to obtain
247 the mtDNA loaded-liposomes. mtDNA loaded-liposomes were equally divided into two aliquots
248 for making VDAC1-containing and VDAC1-free liposomes. Incorporation of purified VDAC1
249 (30 μg/ml) into the mtDNA-loaded liposomes solution was performed by incubating the liposomes
250 with VDAC1 for 20 min at room temperature, followed by three freeze–thaw cycles and mild
251 sonication. VDAC1-free liposomes were similarly prepared by using VDAC1-column elution
252 buffer instead of VDAC1. Samples were centrifuged for 15 min at 100,000×*g* and pellets were re-
253 suspended in buffer (10 mM Tricine, 150 mM NaCl, pH 7.4). Liposomes were diluted fourfold
254 and 40 min later, samples were centrifuged for 15 min at 100,000×*g* and supernatant aliquots were
255 analyzed for mtDNA using qPCR with a mtDNA specific primer of the D-loop3 region (Table.
256 S1C).
257
258 Mitochondrial swelling assay and $Ca^{2+}$ accumulation analysis

259 The mPTP opening was analyzed following mitochondria swelling. Briefly, freshly isolated
260 mitochondria (0.5 mg/ml) were incubated for 2 min at 24°C with the indicated concentrations of
261 VBIT-4 for the $Ca^{2+}$-induced mitochondrial swelling assay. Swelling was initiated by the addition
262 of $Ca^{2+}$ (0.1 mM) to the sample cuvette. Absorbance changes at 520 nm were monitored every 16
263 s for 15 min. Cyclosporine A (10 μM) was used as a positive control. Results are shown as a
264 percentage of control. $Ca^{2+}$ accumulation by freshly isolated rat liver mitochondria (0.5 mg/ml)
265 was assayed with the indicated concentrations of VBIT-4 in the presence of 120 mM $CaCl_2$
266 (containing [$^{45}Ca^{2+}$]), 220 mM mannitol, 70 mM sucrose, 5 mM succinate, 0.15 mM Pi and 15
267 mM Tris/HCl, pH 7.2. $Ca^{2+}$ uptake was terminated by rapid Millipore filtration (0.45 μm) followed
268 by a wash with 5 ml of 0.15 M KCl. Results are shown as a percentage of control.
269
270 VDAC1 cross-linking assay
271 Purified VDAC1 (16 μg/ml) was incubated with 60 nM of mtDNA (120 bp) for 15 min at
272 25°C in 20 mM Tricine, pH 8.4 and then incubated for 15 min at 30°C with the cross-linking
273 reagent EGS (100 μM). Samples were subjected to SDS-PAGE and immunoblotting using anti-
274 VDAC1 antibody (ab154856, abcam). Quantitative analysis of immuno-reactive VDAC1 dimer,
275 trimer and multimer bands was performed using FUSION-FX (Vilber Lourmat, France).
276
277 Caspase 3/7 activity and cell viability assay
278 Caspase activity was assayed using the Caspase-Glo 3/7 luminescent assay kit (Promega) or
279 by immunoblotting as described previously. Cell viability was quantified by a sensitive
280 colorimetric viability assay kit, CCK-8 (Dojindo). The luminescent and absorbance were measured
281 using a microplate reader Cytation 3 (BioTek). For live/dead cell staining, cells were stained with
282 2 μM calcein AM (Green) for live cell staining and 4 μM Ethidium homodimer-1, EthD-1 (Red)

283 for dead-cell staining. The stained cells were observed using a LSM880 confocal microscope
284 (Zeiss) equipped with a 63×/1.4 Plan-Apochromat lens (Zeiss).
285
286 Animal model of SLE
287 All experiments were approved by the ACUC (Animal Care and Use Committee) of the
288 NIH/NHLBI. Female MRL/MpJ-*Fas*$^{lpr}$/J mice (stock #000485) were used as a model to determine
289 the etiology of systemic lupus erythematosus (SLE). MRL/MpJ mice (stock #000486) were used
290 as a control for MRL/MpJ-*Fas*$^{lpr}$/J mice. All mice were purchased from The Jackson Laboratory.
291 VBIT-4 was freshly dissolved in DMSO and diluted in water (final pH 5.0, DMSO 0.05%). The
292 MRL/MpJ-*Fas*$^{lpr}$/J mice were treated with a daily freshly diluted dose of VBIT-4 (20 mg/kg) or
293 vehicle water (final pH 5.0, DMSO 0.05%) in drinking water for 5 w, beginning at 11 w of age
294 until euthanasia at 16 w of age. Blood and urine samples were collected when the mice were 16 w
295 of age. Body weight were measured before and after VBIT-4 administration (11 and 16 w of age
296 respectively). Skin, kidney, thymus, and lymph nodes were also collected.
297
298 Albumin:creatinine ratio in the urine
299 Urinary albumin and creatinine were measured after VBIT-4 administration (16 w of age)
300 using ELISA kits (Exocell) following the manufacturer's instructions to determine the
301 albumin:creatinine ratio.
302
303 Quantification of mtDNA, anti-dsDNA antibodies, anti-nuclear antigen (ANA), and IgG in the
304 serum of animal model of lupus
305 Circulating mtDNA was isolated from 500 μl of the experimental mouse serum collected at
306 16 w of age by using the QIAamp Circulating Nucleic Acid Kit (Qiagen) according to the

307 manufacturer's protocol. In brief, serum samples were incubated with proteinase K and carrier
308 RNA at 55°C for 30 min in lysis buffer, and the circulating nucleic acids were bound to the silica
309 membrane by applying vacuum pressure. After washing, the eluted samples were used for qPCR.
310 Primers from the mtDNA D-loop region were used to quantify serum mtDNA (Table S1C). Anti-
311 dsDNA antibodies were detected in the serum using an ELISA kit (Alpha Diagnostic). ANA were
312 detected using an ANA ELISA Kit (Alpha Diagnostic), and IgG were detected using a total-IgG
313 ELISA Kit (Invitrogen) following the manufacturer's instructions.
314
315 Immune complex deposition in kidney glomeruli
316 Kidneys were harvested from MpJ-*Fas*$^{lpr}$ mice. Frozen kidney sections were fixed in cold
317 acetone for 20 min, washed, and blocked for 18 h at 4°C with 4% BSA in PBS. To detect
318 glomerular deposits, the sections were stained with FITC-conjugated anti-mouse C3 antibody
319 (GC3-90F-Z, Immunology Consultants Laboratory) and Alexa Fluor 594-conjugated anti-Mouse
320 IgG antibody (A-11020, Invitrogen) with 1 μg/ml of Hoechst 33342 (Life Technologies) staining
321 for 1 h at room temperature. After washing with PBS, the tissues were mounted, and the slides
322 were observed using a LSM880 confocal microscope (Zeiss). The fluorescence intensity score was
323 determined after analyzing random images for each animal in a blinded manner.
324
325 Human samples and study approval
326 Heparinized venous peripheral blood was obtained from SLE subjects or from healthy
327 controls enrolled at the Clinical Center, National Institutes of Health. All individuals signed an
328 informed consent form following IRB-approved protocols (NIH 94-AR-0066). SLE subjects
329 fulfilled the revised American College of Rheumatology diagnostic criteria (*6*). Disease activity

330 was determined using the SLEDAI-2K criteria (*7*). Individuals with recent or active infections
331 were excluded.
332
333 Isolation of normal-density granulocytes and low-density granulocytes
334 Human normal-density granulocytes (NDGs) were isolated from heparinized venous blood
335 using a Ficoll-Paque gradient (GE Healthcare) with dextran (Sigma-Aldrich) sedimentation,
336 followed by red blood cell lysis using hypotonic NaCl as described previously (*8*). LDGs were
337 isolated from the PBMC layer using a negative-selection method as described previously (*8*).
338
339 Visualization and quantification of Neutrophil extracellular traps
340 Neutrophil extracellular traps (NETs) were induced in NDGs by incubating human
341 granulocytes with the calcium ionophore A23187 (25 μM) (Thermo Fisher) in RPMI 1640 medium
342 for 2 h. NETs were then quantified as previously described (*9*) using SYTOX fluorescent dye at
343 485/520 nm to quantify extracellular DNA. The fluorescence of PicoGreen (Life Technologies) at
344 t = 0 min was measured at 485/520 nm (emission/extinction) to quantify the total DNA. The
345 fluorescence was quantified using a microplate reader Synergy HTX (BIOTEK). NETs were also
346 quantified by fluorescence microscopy as previously described (*9*). In brief, the cells were attached
347 to coverslip chambers, stimulated for 90 min at 37°C with A23187 (25 μM), fixed with 4%
348 paraformaldehyde overnight at 4°C, and permeabilized with 0.2% Triton X-100 for 10 min,
349 followed by 0.5% gelatin for 20 min. The cells were stained with primary antibodies against human
350 neutrophil elastase (ab21595, abcam) for 2 h at room temperature, washed in PBS, and stained
351 with 1 μg/ml of Hoechst 33342 (Life Technologies) and Alexa Fluor 488-conjugated secondary
352 antibody (A31570, Life Technologies) against the primary antibodies for 2 h at room temperature.

353 After mounting, the cells were visualized with a LSM880 confocal microscope (Zeiss) equipped
354 with a 63×/1.4 Plan-Apochromat lens (Zeiss).
355
356 Statistical analyses
357 Statistical comparisons between groups were performed by two-tailed unpaired Student's *t*-test
358 and ANOVA with Tukey's post-hoc test for multiple comparisons using GraphPad Prism7
359 software (GraphPad). For the statistical analyses of human samples, the sample size was
360 determined using similar patient numbers per experimental condition. The normality distribution
361 of the sample sets was determined by the d'Agostino and Pearson omnibus normality test. For
362 sample sets with a Gaussian distribution, Student's two-tailed *t*-test, paired *t*-test, or Pearson's
363 correlation coefficient analysis was performed. For the limited number of sample sets with a non-
364 Gaussian distribution, the Mann–Whitney *U* test was performed as applicable. Multiple
365 comparisons with the same group in more than one analysis were adjusted using the Bonferroni
366 correction. All values are presented as the mean ± SEM of at least three independent experiments,
367 and differences were considered statistically significant at $p < 0.05$.
368

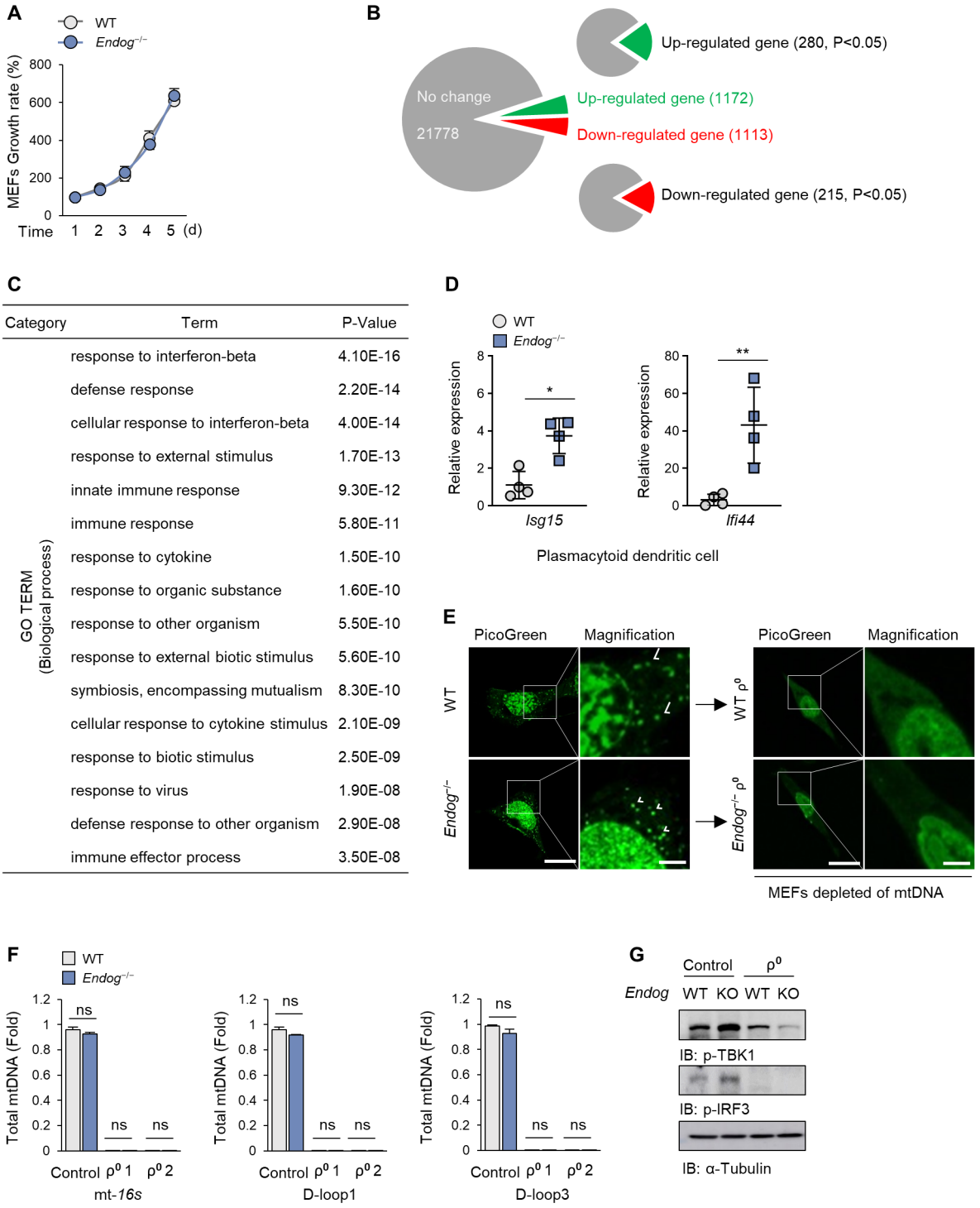


| Category | Term | P-Value |
|---|---|---|
| GO TERM (Biological process) | response to interferon-beta | 4.10E-16 |
| | defense response | 2.20E-14 |
| | cellular response to interferon-beta | 4.00E-14 |
| | response to external stimulus | 1.70E-13 |
| | innate immune response | 9.30E-12 |
| | immune response | 5.80E-11 |
| | response to cytokine | 1.50E-10 |
| | response to organic substance | 1.60E-10 |
| | response to other organism | 5.50E-10 |
| | response to external biotic stimulus | 5.60E-10 |
| | symbiosis, encompassing mutualism | 8.30E-10 |
| | cellular response to cytokine stimulus | 2.10E-09 |
| | response to biotic stimulus | 2.50E-09 |
| | response to virus | 1.90E-08 |
| | defense response to other organism | 2.90E-08 |
| | immune effector process | 3.50E-08 |

**Fig. S1. Interferon response in *Endog*$^{-/-}$ MEFs.** (**A**) cell growth rate in WT and *Endog*$^{-/-}$ MEFs. (**B**) ISG expression levels in WT and *Endog*$^{-/-}$ plasmacytoid dendritic cells. (**C** and **D**) RNAseq

372 analysis in WT and *Endog*$^{-/-}$ MEFs. Schematic pie charts indicate statistically upregulated and
373 downregulated genes in *Endog*$^{-/-}$ versus WT MEFs (C). Gene ontology analysis of upregulated
374 genes (D). (**E** and **F**) WT and *Endog*$^{-/-}$ $\rho^0$ MEFs were devoid of mtDNA. Nuclear and
375 mitochondrial DNA in MEFs were stained by PicoGreen, and white arrowheads indicate mtDNA.
376 Scale bar, 40 μm; magnification, 10 μm. (E). Total mtDNA levels in WT and *Endog*$^{-/-}$ MEFs as
377 well as two independently-generated $\rho^0$ MEFs ($\rho^0$ 1 and $\rho^0$ 2), from both WT and *Endog*$^{-/-}$ MEFs
378 (F). (**G**) Phosphorylation of TBK and IRF3 was visualized in $\rho^0$ MEFs derived from WT and
379 *Endog*$^{-/-}$ MEFs and their controls by immunoblotting. All values are presented as the mean ± SEM
380 of at least three independent experiments. *$p < 0.05$; **$p < 0.01$; ns, not significant.
381

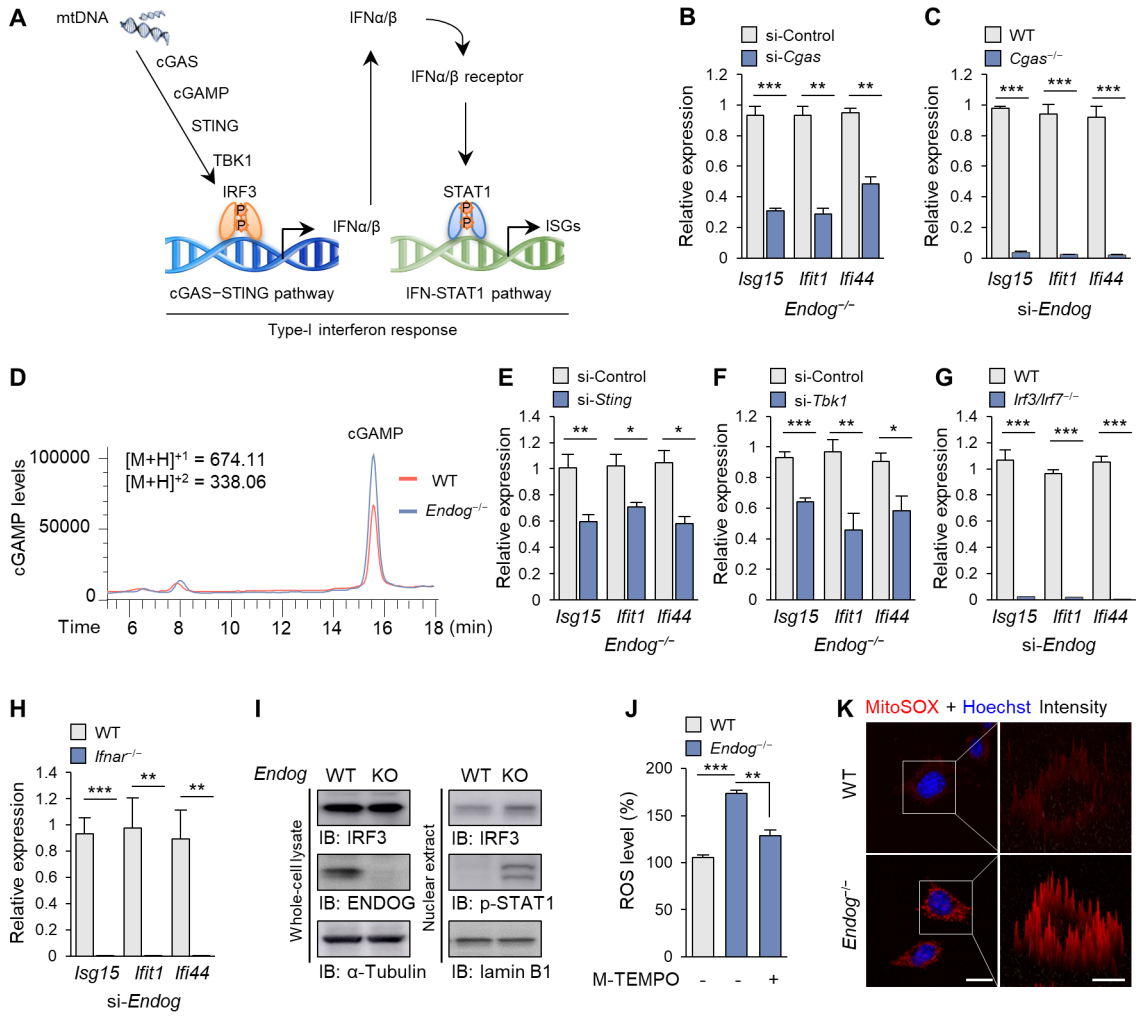


382

383 **Fig. S2. ROS-mediated cmtDNA activates the cGAS–STING pathway.** (**A**) Schematic diagram
384 of the cGAS–STING cytosolic DNA sensing pathway and the IFN/STAT1 pathway for ISG
385 expression. cGAS, which generates the cyclic dinucleotide cGAMP upon binding to cytosolic
386 DNA, is a key effector of the type-I IFN response. (**B** to **G**) The cGAS–STING pathway in
387 *Endog*$^{-/-}$ MEFs. *Endog*$^{-/-}$ MEFs transfected with siRNA for *Cgas* (B) and *Endog* siRNA was
388 transfected into *Cgas*$^{-/-}$ MEFs (C). Intracellular levels of cGAMP were determined by LC/MS in
389 WT and *Endog*$^{-/-}$ MEFs (D). *Endog*$^{-/-}$ MEFs transfected with siRNA for *Sting* (E), or *Tbk1* (F),
390 *Endog* siRNA was transfected into *Irf3/Irf7*$^{-/-}$ MEFs (G). (**H** and **I**) IFN/STAT1 pathway in
391 *Endog*$^{-/-}$ MEFs. *Endog* siRNA was transfected into *Ifnar*$^{-/-}$ MEFs (H). WT and *Endog*$^{-/-}$ MEFs

392 were fractionated and whole-cell lysate and nuclear extract were subjected to immunoblotting,
393 using the indicated antibodies (I). (**J**) mROS levels were measured in WT and *Endog*$^{-/-}$ MEFs
394 after treatment with Mito(M)-TEMPO (10 μM) for 48 h. (**K**) Confocal microscopy images of
395 MitoSOX (mitochondria) and Hoechst (Nucleus). Scale bar, 20 μm; magnification, 10 μm. All
396 values are presented as the mean ± SEM of at least three independent experiments. *$p < 0.05$; **$p$
397 $< 0.01$; ***$p < 0.005$.
398

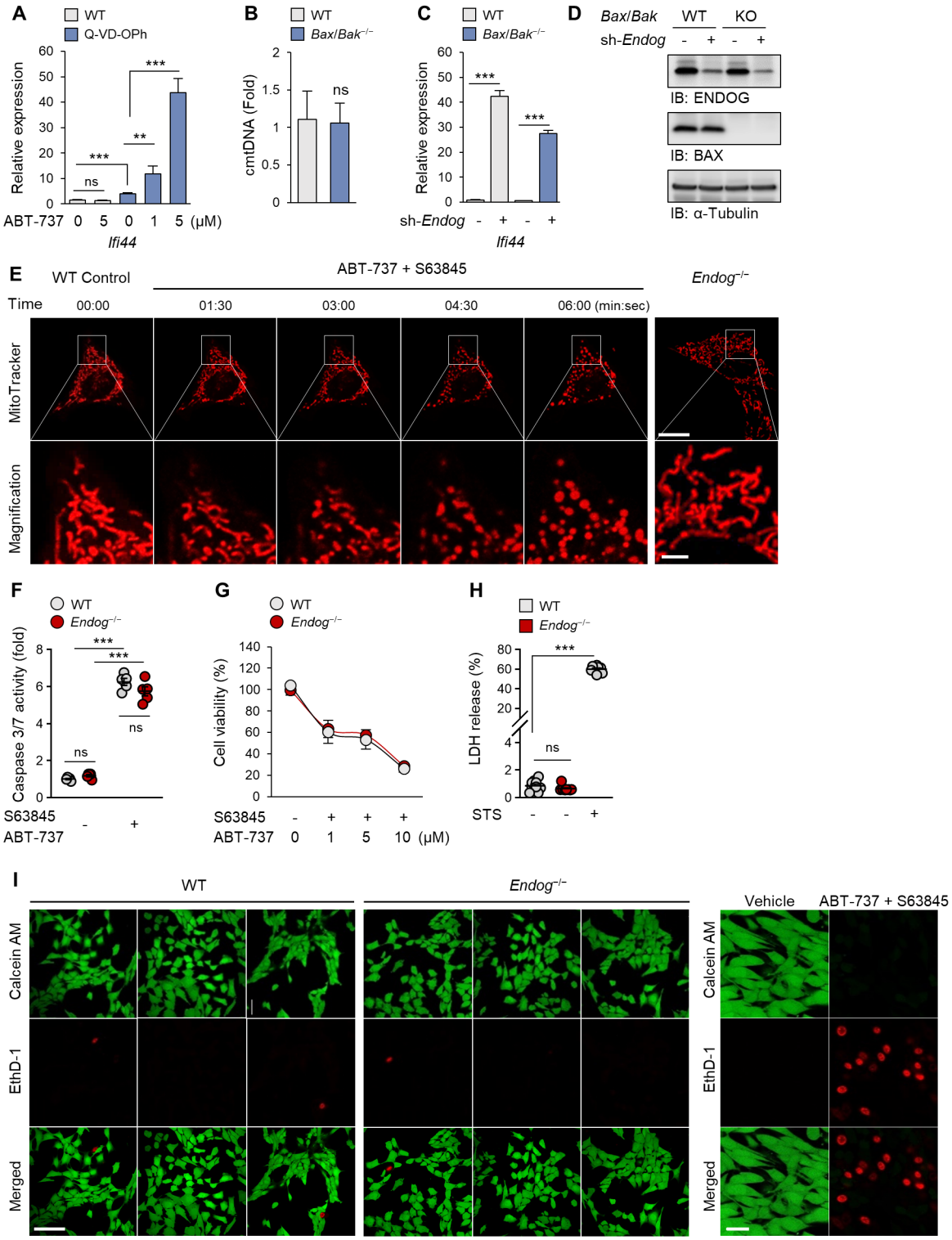
A
WT
Q-VD-OPh
Relative expression
ABT-737 0 5 0 1 5 (μM)
Ifi44
B
WT
Bax/Bak−/−
cmtDNA (Fold)
ns
C
WT
Bax/Bak−/−
Relative expression
sh-Endog - + - +
Ifi44
D
Bax/Bak WT KO
sh-Endog - + - +
IB: ENDOG
IB: BAX
IB: α-Tubulin
E
WT Control
ABT-737 + S63845
Endog−/−
Time 00:00 01:30 03:00 04:30 06:00 (min:sec)
MitoTracker
Magnification
F
WT
Endog−/−
Caspase 3/7 activity (fold)
S63845 - +
ABT-737
G
WT
Endog−/−
Cell viability (%)
S63845 - + + +
ABT-737 0 1 5 10 (μM)
H
WT
Endog−/−
LDH release (%)
STS - - +
I
WT
Endog−/−
Vehicle
ABT-737 + S63845
Calcein AM
EthD-1
Merged

399

400 **Fig. S3. *Endog*-deficiency does not increase apoptosis.** (**A**) The ISG expression level was
401 measured in WT MEFs after activation of BAX/BAK with the BCL-2 inhibitor ABT-737 in the
402 presence of the caspase inhibitor Q-VD-OPh (10 μM). Q-VD-OPh was used because apoptotic
403 caspases suppress mtDNA-induced ISG expression. (**B**) cmtDNA levels in WT and *Bax/Bak*$^{-/-}$
404 MEFs. (**C** and **D**) ISG expression levels were measured after knocking down *Endog* in WT and
405 *Bax/Bak*$^{-/-}$ MEFs by RT-qPCR (C). Expressed levels of ENDOG and BAX are shown by
406 immunoblotting (D). (**E**) Time lapse image of WT mitochondrial morphology after induction of
407 apoptosis with a combination of ABT-737 (10 μM) and the MCL-1 inhibitor S63845 (5 μM) in
408 the presence of the caspase inhibitor Q-VD-OPH (10 μM), and mitochondrial morphology of
409 *Endog*$^{-/-}$ MEFs. Scale bar, 20 μm; magnification, 5 μm. (**F** and **G**) Caspase 3/7 activity of WT and
410 *Endog*$^{-/-}$ MEFs treated with ABT-737 (10 μM) and S63845 (5 μM) for 4 h (F) and Viability of
411 MEFs for 24 h (G). (**H**) LDH release in WT and *Endog*$^{-/-}$ MEF. Treatment with apoptosis inducer
412 staurosporin (STS) (2 μM) was used as a positive control for LDH release. (**I**) Viability of WT and
413 *Endog*$^{-/-}$ MEFs by live (calcein-AM) or dead (ethidium homodimer-1, EthD-1) staining. Scale bar,
414 100 μm. (left). Treatment with ABT-737 (10 μM) and S63845 (5 μM) were used as a positive
415 control for apoptosis. Scale bar, 20 μm. (right). All values are presented as the mean ± SEM of at
416 least three independent experiments. **$p < 0.01$; ***$p < 0.005$; ns, not significant.
417

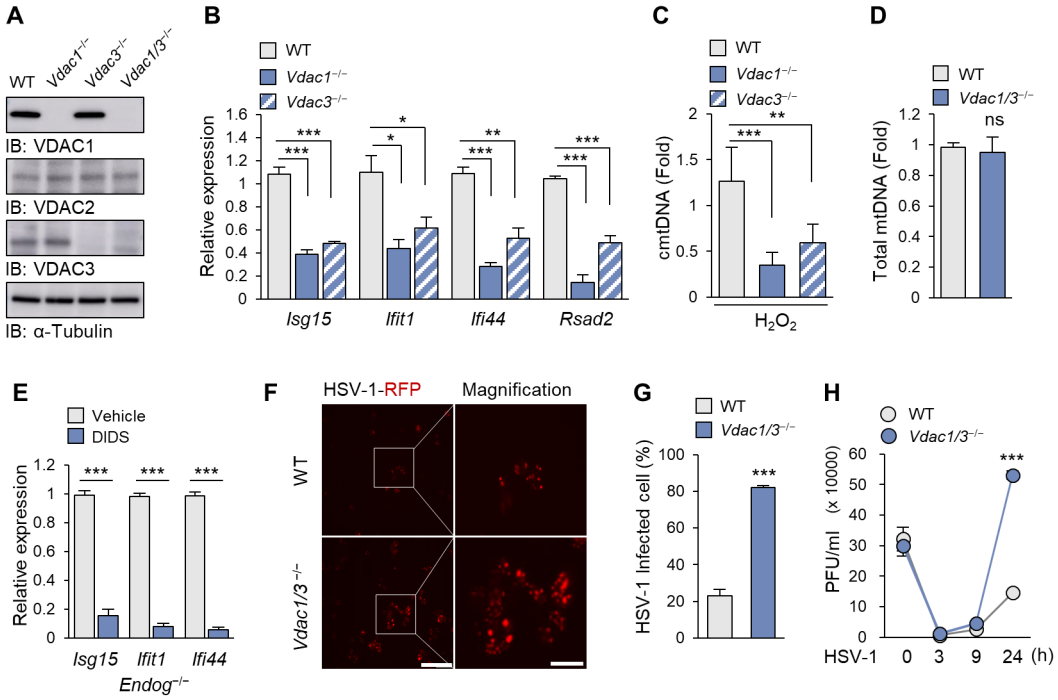


**Fig. S4. The roles of VDAC in the type-I interferon response.** (**A**) Expression level of VDAC isoforms in *Vdac1*$^{-/-}$, *Vdac3*$^{-/-}$ and *Vdac*1/3 $^{-/-}$ MEFs were visualized by immunoblotting. (**B** to **D**) ISG expression levels (B), cmtDNA levels (C), and total mtDNA levels (D) were measured by RT-qPCR. (**E**) ISG expression levels were determined after treatment with 4,4'-diisothiocyanostilbene-2,2'-disulfonic acid (DIDS) (100 μM) for 24 h in *Endog*$^{-/-}$ MEFs by RT-qPCR. (**F** to **H**) HSV-1-red fluorescent protein (RFP) infection in WT and *Vdac1/3*$^{-/-}$ MEFs (MOI=0.1). Scale bar, 100 μm; magnification, 30 μm. (F). Percentage of RFP positive cells were determined by flow cytometry (G). The replication kinetics of HSV-1-RFP was determined by measuring the virus growth curve. Virus titers were then determined in Vero cells (H). All values are presented as the mean ± SEM of at least three independent experiments. *$p < 0.05$; **$p < 0.01$; ***$p < 0.005$; ns, not significant.

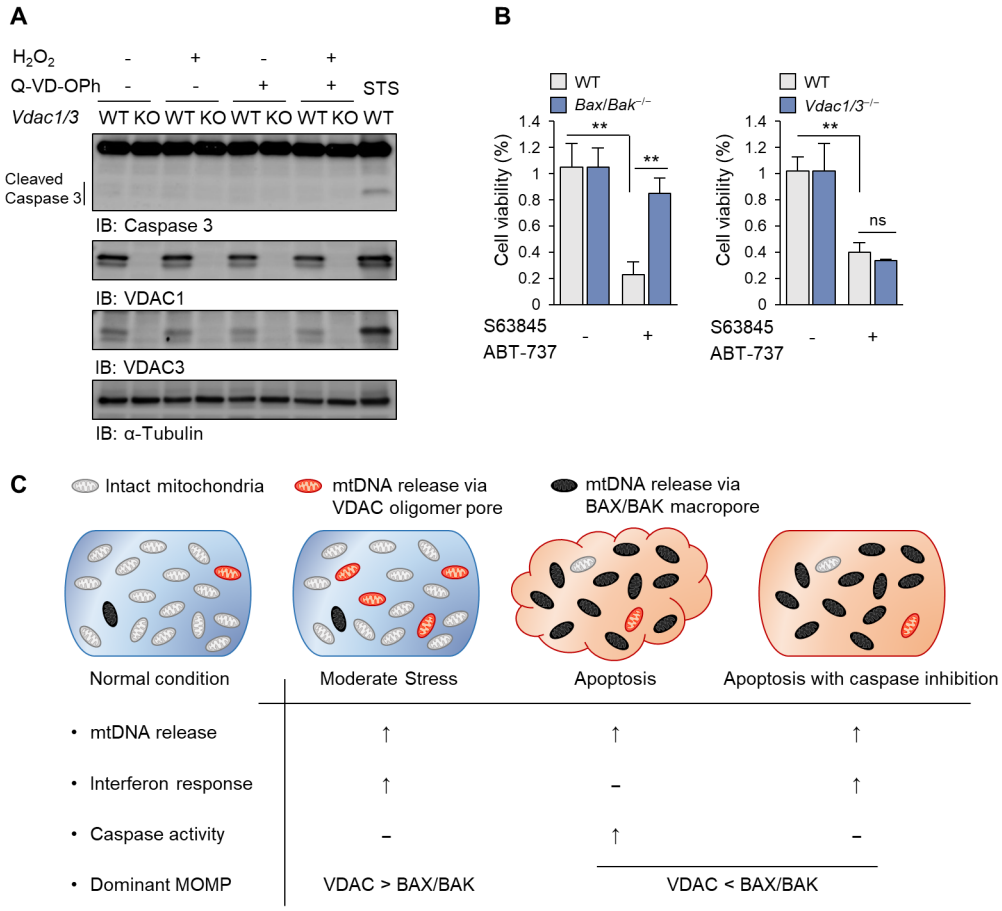


431

432 **Fig. S5. The roles of VDAC on apoptosis.** (**A**) Caspase 3 cleavage in WT and V*dac1/3*$^{-/-}$ MEFs
433 after treatment with or without $H_2O_2$ (100 μM) and/or Q-VD-OPh (10 μM) for 24 h was visualized
434 by immunoblotting. STS (2 μM) was used as a positive control for caspase 3 cleavage. (**B**)
435 Viability of WT, *Bax/Bak*$^{-/-}$ and *Vdac1/3*$^{-/-}$ MEFs treated with ABT-737 (10 μM) and S63845 (5
436 μM) for 24 h. (**C**) Schematic diagram of mtDNA release, interferon response, and caspase activity
437 in stressed conditions in comparison to normal conditions. All values are presented as the mean ±
438 SEM of at least three independent experiments. **$p < 0.01$; ns, not significant.

439

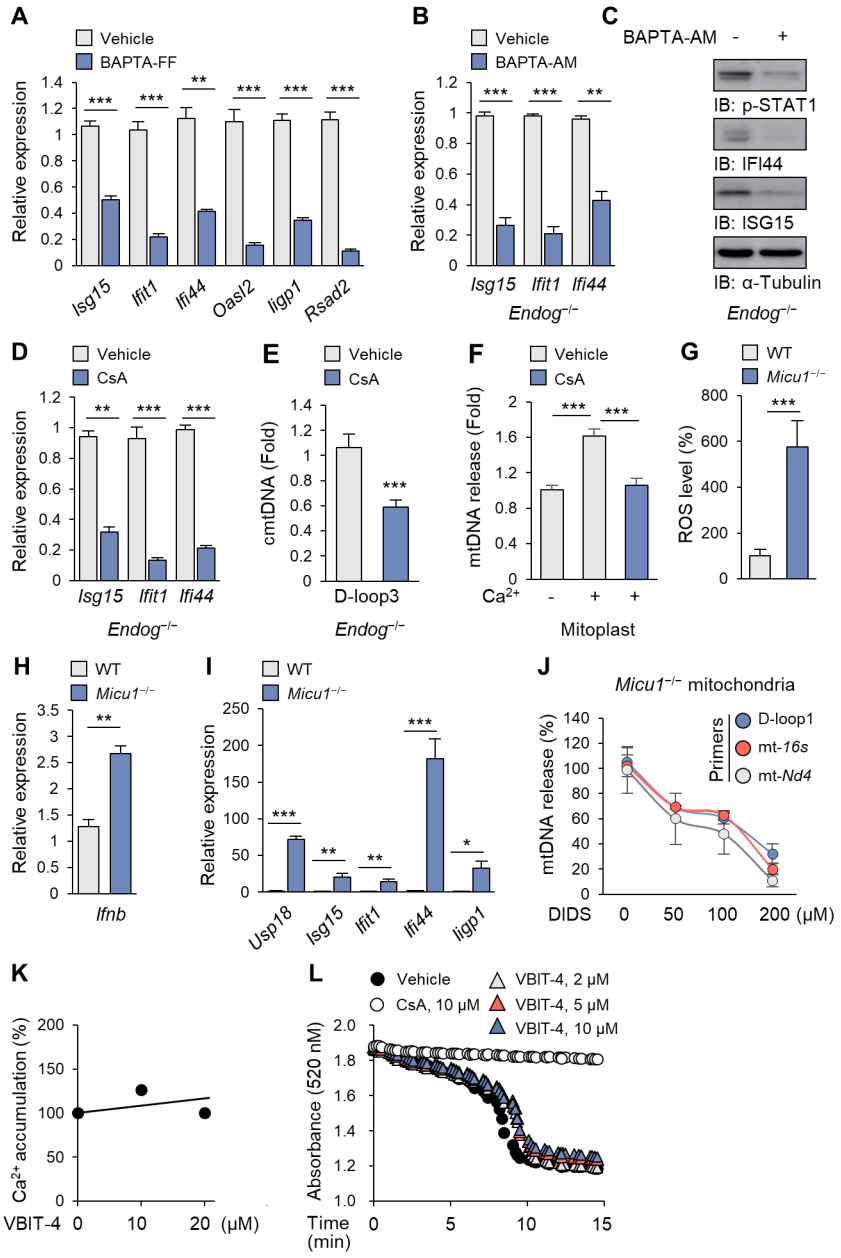


440

441 **Fig. S6. The role of $Ca^{2+}$ and mPTP in mtDNA release in live cells.** (**A** to **C**) ISG expression

442 levels were measured in *Endog*$^{-/-}$ MEFs after treatment with the calcium chelators BAPTA-FF

443 (15 μM) (A) and BAPTA-AM (20 μM) (B) by RT-qPCR and immunoblot (C). (**D**) ISG

444 expression levels were measured in *Endog*$^{-/-}$ MEFs after treatment with Cyclosporine A (CsA).

445 (**E**) cmtDNA levels were measured after treatment with CsA. (**F**) Levels of released mtDNA

446 were measured in mitoplasts after treatment with $Ca^{2+}$ and CsA. (**G**) ROS levels were detected
447 by using the CM-$H_2$DCFDA probe in WT and *Micu1*$^{-/-}$ MEFs. (**H** and **I**) *Ifnb* (H) and ISG (I)
448 expression levels were evaluated in WT and *Micu1*$^{-/-}$ MEFs. (**J**) The effect of VDAC inhibitor
449 DIDS on mtDNA released from isolated mitochondria from *Micu1*$^{-/-}$ MEFs during incubation in
450 a buffer without $Ca^{2+}$ (qPCR was performed using the three indicated primers). (**K**) Effect of
451 VBIT-4 on $Ca^{2+}$ accumulation in freshly isolated mitochondria. (**L**) $Ca^{2+}$-induced mitochondrial
452 swelling was assayed in freshly prepared mitochondria in the presence of varying concentrations
453 of VBIT-4. All values are presented as the mean ± SEM of at least three independent
454 experiments. *$p < 0.05$; **$p < 0.01$; ***$p < 0.005$.
455

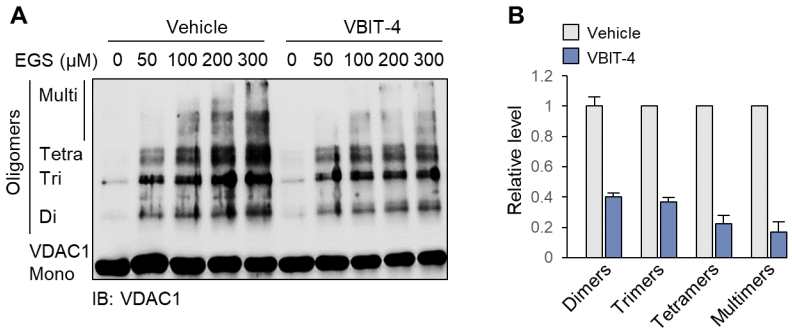


456

457 **Fig. S7. VDAC1 oligomerization in liposomes.** (**A**) The effect of VBIT-4 on VDAC1
458 oligomerization in liposome. Purified rat liver VDAC1 was reconstituted into liposomes as in Fig.
459 2F and incubated with or without VBIT-4 (20 μM) for 30 min. VDAC1 was then crosslinked using
460 the indicated concentrations of EGS before immunoblotting. The positions of VDAC1 monomers
461 (Mono), dimers (Di), trimers (Tri), tetramers (Tetra) and multimers (Multi) are indicated. (**B**)
462 Quantification of VDAC1 oligomers shown in (A).

463

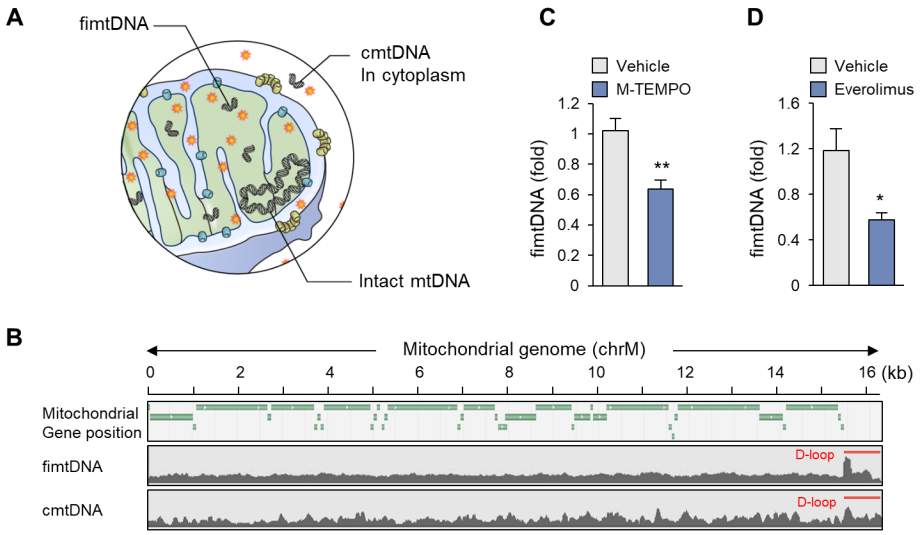


464

465 **Fig. S8. The distribution of fimtDNA and cmtDNA fragments.** (**A**) Schematic diagram of
466 mitochondria containing intact mtDNA, fimtDNA, and cmtDNA. (**B**) The distribution of fimtDNA
467 and cmtDNA fragments that were visualized by Integrated Genome Browser. The results shown
468 are the average of three samples. Green boxes indicate mitochondrial gene positions, and red lines
469 indicate the D-loop region. (**C** and **D**) qPCR analysis of the fimtDNA by treatment with 10 μM
470 Mito-TEMPO (C) and 100 nM mTORC1 inhibitor everolimus (D) for 48 h. All values are
471 presented as the mean ± SEM of at least three independent experiments. *$p < 0.05$; **$p < 0.01$.

472

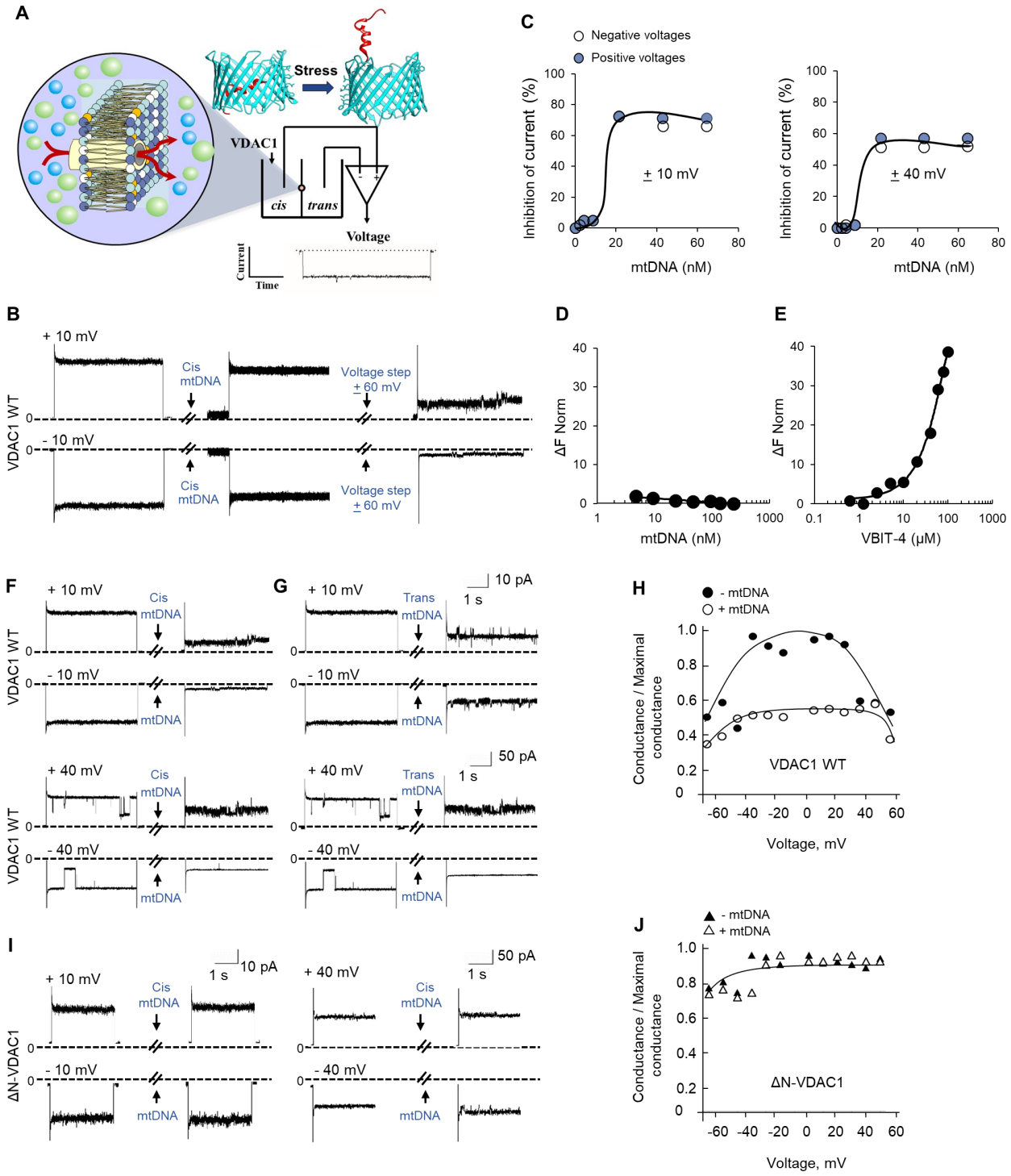


**Fig. S9. The effects of mtDNA on VDAC1 and ΔN-VDAC1 conductance.** (**A**) Schematic diagram of channel conductance properties assay by reconstitution of VDAC1 into a planar lipid bilayer (PLB). VDAC1 is composed of 19 transmembrane β-strands forming a membrane-

477 embedded β-barrel and a flexible amphipathic 26-residue-long N-terminal domain that lies inside
478 the channel but can translocate from within the channel to the pore surface when VDAC1
479 oligomerizes. As mtDNA fragments pass through the VDAC1 oligomer pores, direct mtDNA–
480 VDAC1 interaction may occur. In order to test this, purified mitochondrial VDAC1 was
481 reconstituted into PLB and the effect of mtDNA fragments on channel conductance under voltage-
482 clamp conditions was measured. (**B**) Single channel current through VDAC1 was recorded in
483 response to voltage steps 0 to 10 mV or –10 mV. Next, mtDNA was added to the cis side of the
484 PLB and channel conductance was recorded 2–5 min following mtDNA addition. After about 20
485 min, the channel was exposed to a high voltage step and current through the channel was recorded
486 at ± 10 mV. The dashed lines indicate the zero-level current. mtDNA inhibited VDAC1
487 conductance, but it required pre-exposure of the PLB-reconstituted channel to a high voltage (60
488 mV). Evidence suggests that high voltage exposes the VDAC1 N-terminal domain by inducing its
489 translocation out of the VDAC1 potentially allowing its interaction with mtDNA. (**C**)
490 Concentration-dependent inhibition of VDAC1 channel conductance by mtDNA (the cis
491 compartment) at ± 10 mV and ± 40 mV. (**D** and **E**) Analysis of mtDNA (D) or VBIT-4 (E)
492 interaction with VDAC1 using micro-scale thermophoresis, which cannot be performed with prior-
493 exposure to high voltage for technical reasons, revealed no interaction of mtDNA with VDAC1,
494 whereas VBIT-4 did show interaction with VDAC1. (**F** and **G**) Effect of mtDNA on the
495 conductance of VDAC1. Inhibition of PLB-reconstituted VDAC1 conductance by mtDNA is
496 shown before and after the addition of mtDNA in the cis; cytoplasm facing side (F) or trans;
497 intermembrane space side (G) compartment at ± 10 mV and ± 40 mV. Samples were pre-exposed
498 to 60 mV before the conductance measurement. (**H**) Effect of mtDNA on VDAC1 channel
499 conductance as a function of voltage, from 60 mV to –60 mV. (**I** and **J**) Effect of mtDNA on
500 channel conductance of PLB-reconstituted ΔN-VDAC1. Channel conductance was measured

501 before and after the addition of mtDNA in the cis compartment at ± 10 mV and ± 40 mV. Samples
502 were pre-exposed to 60 mV before the conductance measurement. Effects of mtDNA on ΔN-
503 VDAC1 relative conductance as a function of voltage, from 60 mV to –60 mV (J). Relative
504 conductance (conductance/maximal conductance) was determined as the average steady-state
505 conductance at a given voltage normalized to the conductance at 10 mV, maximal conductance.
506

**A**

| Peptide sequence alignment | Species | |
|---|---|---|
| MAVPPTYADLGKSARDVFTKGYGFGL | Human | Homo sapiens |
| MAVPPTYADLGKSARDVFTKGYGFGL | Mouse | Mus musculus |
| MAVPPTYADLGKSARDVFTKGYGFGL | Rat | Rattus norvegicus |
| MAVPPTYADLGKSARDVFTKGYGFGL | Monkey | Macaca mulatta |
| MAVPPTYADLGKSARDVFTKGYGFGL | Chimpanzee | Pan troglodytes |
| MAVPPTYADLGKSARDVFTKGYGFGL | Sheep | Ovis aries |

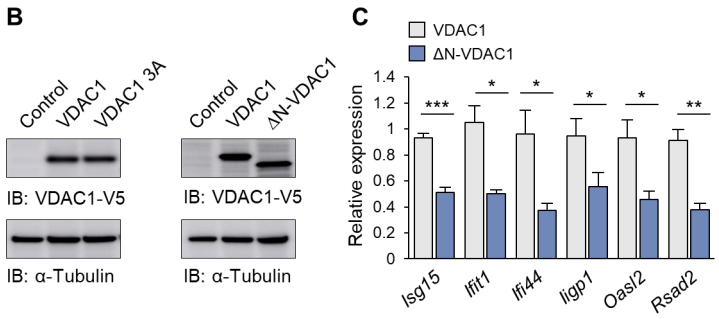


507

508 **Fig. S10. The function of VDAC1 N-terminal region in type-I IFN response.** (**A**) Phylogenetic
509 analysis of VDAC1 N-terminal region. (**B**) VDAC1 and VDAC1 mutant expression levels by
510 immunoblotting. (**C**) ISG expression levels were measured by RT-qPCR in WT and ΔN-VDAC1
511 expressing MEFs after treatment with $H_2O_2$ (100 μM) for 18 h. All values are presented as the
512 mean ± SEM of at least three independent experiments. *$p < 0.05$; **$p < 0.01$; ***$p < 0.005$.

513

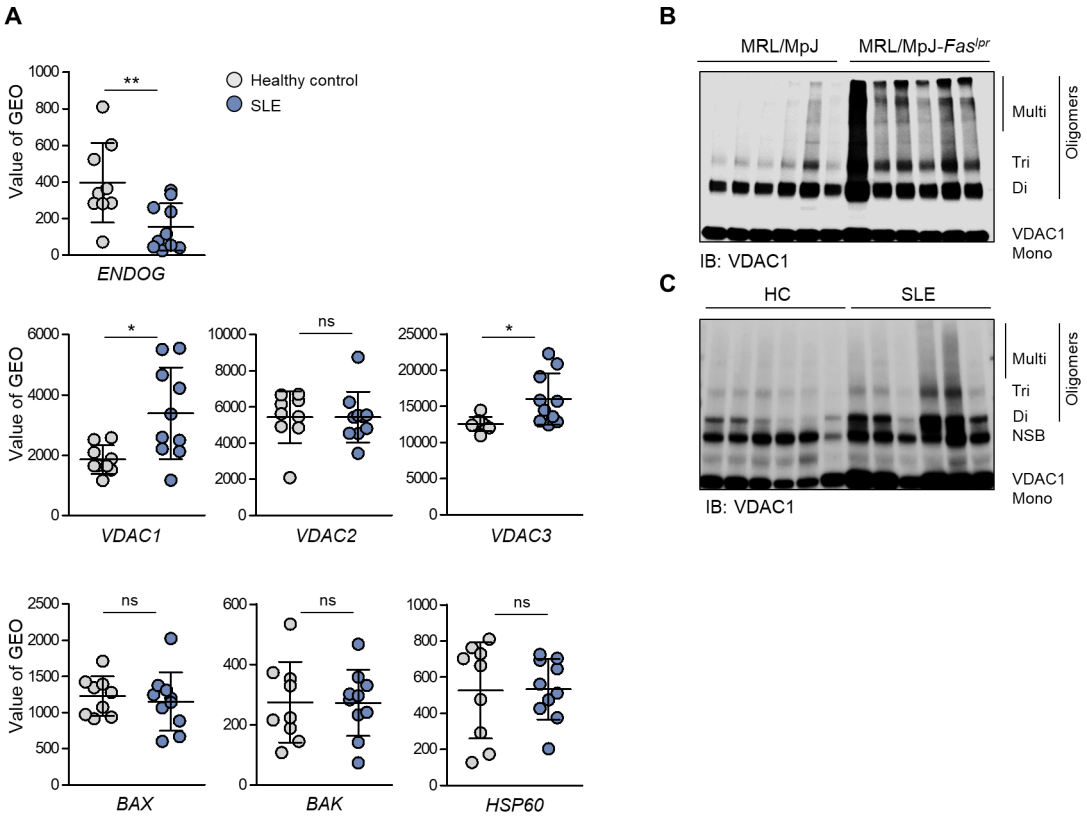


514

515 **Fig. S11. The expression and oligomerization of VDAC1 in lupus-like disease**. (**A**) Analysis
516 of gene expression levels from healthy control and SLE (Lupus) patients. Raw data were obtained
517 from GEO accession no. GSE13887. (**B** and **C**) VDAC1 oligomerization in mouse splenocytes (B)
518 and human PBMC (C) was visualized by immunoblotting (n=6 individuals). NSB, non-specific
519 band.

520

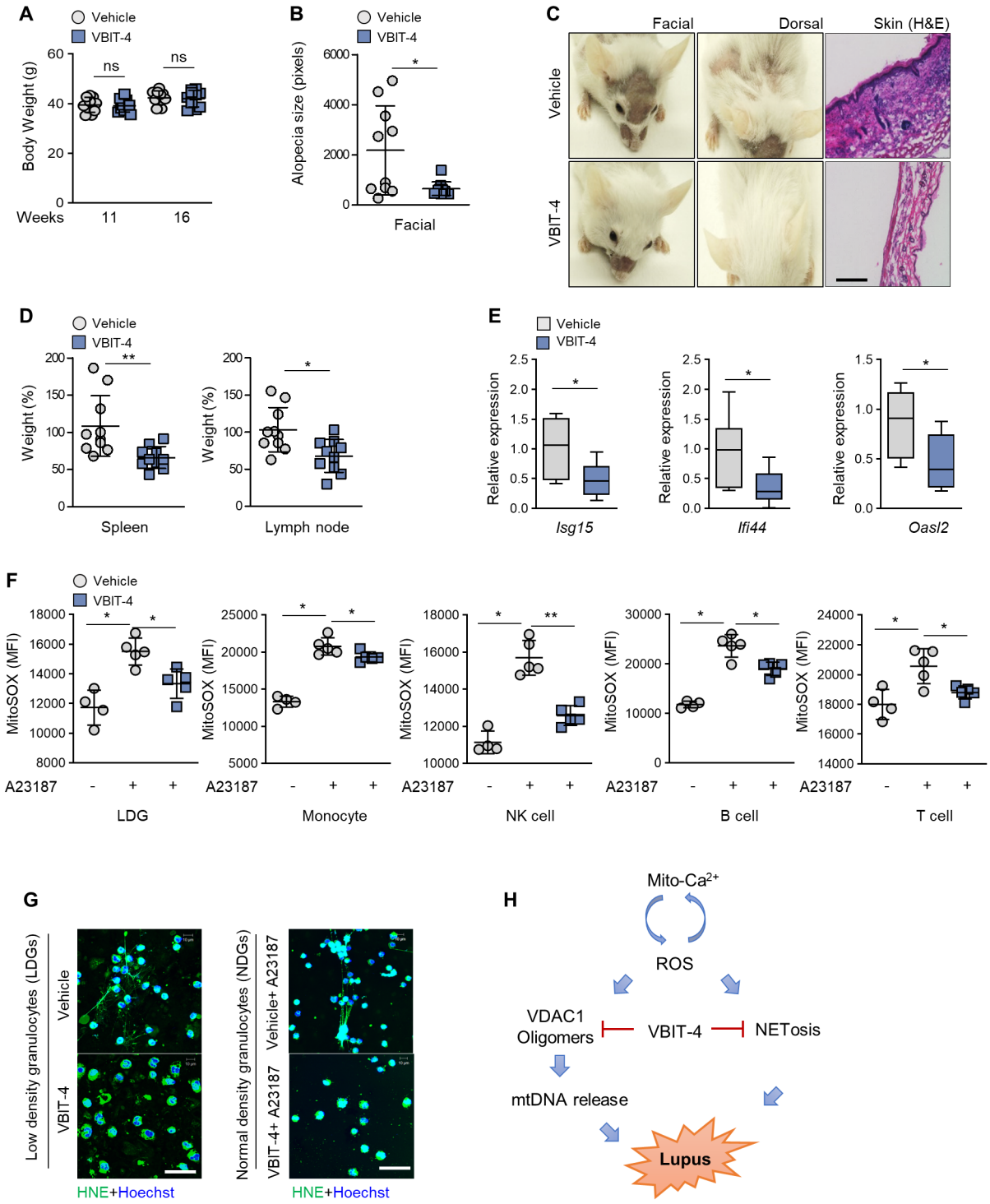


521

522 **Fig. S12. The role of VDAC1 oligomerization in lupus-like disease.** (**A**) Body Weight of vehicle

523 and VBIT-4 treated mice (MpJ-*Fas*$^{lpr}$), at 11 and 16 weeks of age (n=10 in each group). (**B** and **C**)

524 Alopecia in the facial and dorsal areas and erythema in the skin lesions (H&E) of VBIT-4-treated
525 MpJ-*Fas*$^{lpr}$ mice. Quantification of alopecia of the mice (n=10 in each group). (**D**) Weight of the
526 spleen and lymph nodes of treated mice (n=10 in each group). (**E**) Expression of ISG in the spleen
527 of treated mice. (n=6 in each group). (**F**) mROS level was measured by flow cytometry in several
528 cell types after treatment with A23187 and VBIT-4. (**G**) Inhibition of spontaneous NET formation
529 of low-density granulocytes (LDGs, SLE) by VBIT-4. Scale bar, 40 μm (left). Inhibition of
530 A23187-stimulated NET formation of normal-density granulocytes (NDGs, SLE) by VBIT-4.
531 Scale bar, 40 μm (right). Green represents human neutrophil elastase (HNE), and blue represents
532 DNA (Hoechst). (**H**) Schematic diagram of development of lupus-like disease by VDAC1. VBIT-
533 4, which inhibits VDAC1 oligomerization, decreases mtDNA release, type-I IFN signaling,
534 neutrophil extracellular traps (NETs) and disease severity in SLE. All values are presented as the
535 mean ± SEM. *$p < 0.05$; **$p < 0.01$; ns, not significant.
536

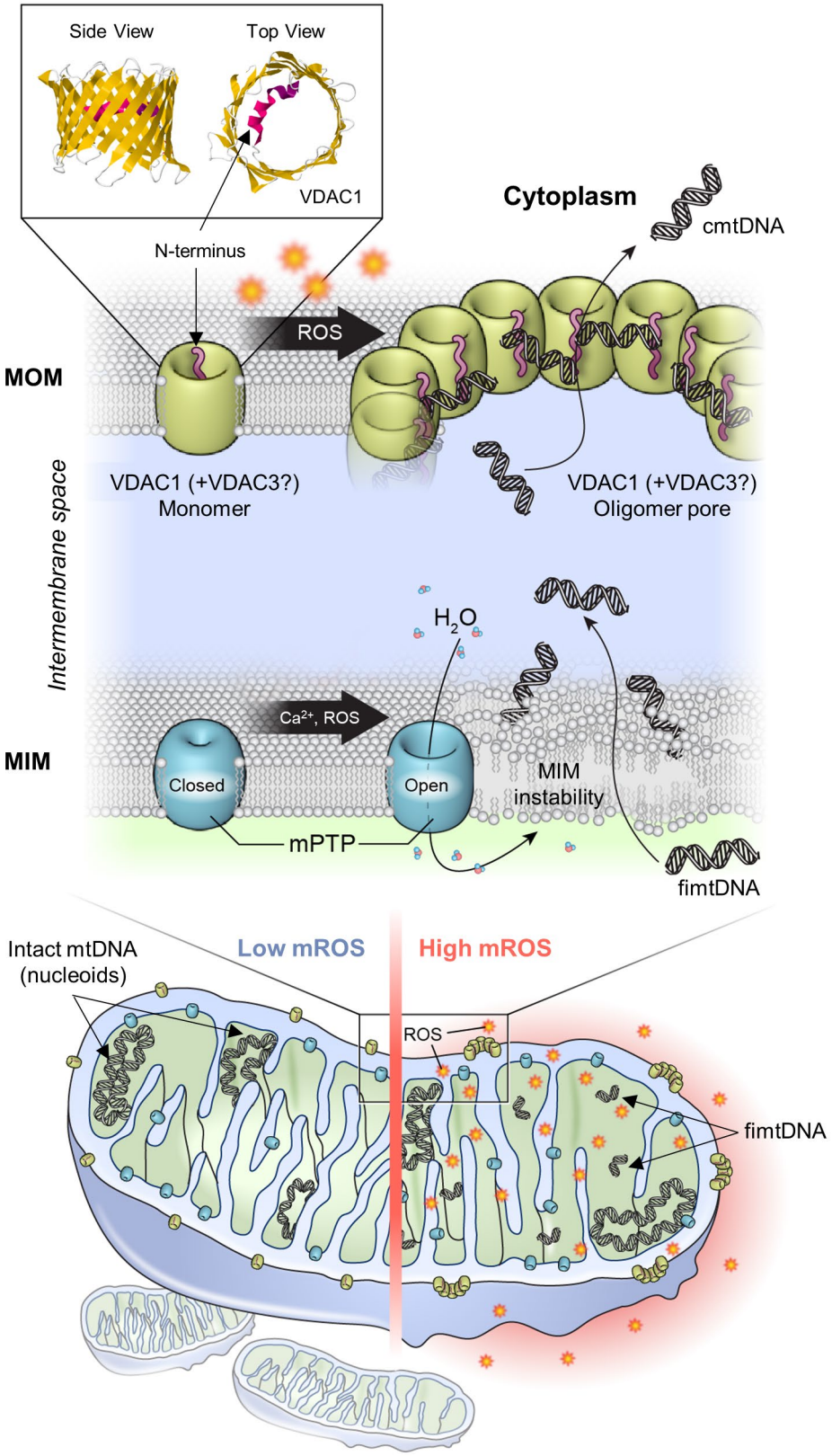
Side View
Top View
VDAC1
N-terminus
Cytoplasm
cmtDNA
ROS
MOM
VDAC1 (+VDAC3?)
Monomer
VDAC1 (+VDAC3?)
Oligomer pore
Intermembrane space
$H_2O$
$Ca^{2+}$, ROS
MIM
Closed
Open
MIM
instability
mPTP
fimtDNA
Intact mtDNA
(nucleoids)
Low mROS
High mROS
ROS
fimtDNA

537

538 **Fig. S13. Schematic diagram of mtDNA release and development of lupus-like disease.** The
539 MOMP created by mROS-induced oligomerization of VDAC1, and possibly VDAC3, releases
540 mtDNA into the cytosol. The highly dynamic N-terminal domain of VDAC translocates out of the
541 channel when VDAC is in an oligomerized state. Unlike the lipophilic β-barrel of VDAC1, the N-
542 terminal α-helix domain is hydrophilic which generates a hydrophilic surface in the oligomer pore
543 and facilitates the passage of mtDNA across the MOM. In our model, the negatively charged
544 backbones of mtDNA fragments interact with the positively charged residues of the VDAC1 N-
545 terminal domain and act as a scaffold to stabilize VDAC1 oligomers. The opening of mPTP in the
546 subpopulation of stressed mitochondria damages MIM, allowing fimtDNA to pass through. The
547 mPTP opening is dependent on $Ca2^{+}$-influx but not on VDAC1 oligomerization. Although
548 VDAC3 is not amenable for in vitro studies because it tends to form aggregations in vitro, it has
549 similar positively-charged residues in its N-terminal domain, overall structure and binding affinity
550 to VBIT-4 (*10*) as VDAC1, suggesting that it may form oligomer pores in a manner similar to
551 VDAC1.
552

**Table S1. Primers and oligos sequence used in this study.**

**A. Primers sequence for VDAC1 mutation.**

| Name | Forward Primer | Reverse Primer |
|---|---|---|
| ΔN-VDAC1 | 5'-AACGGATCCATGATAAAACTTGATTTGAAAAC-3' | 5'-AAGCTCGAGTGCTTGAAATTCCAGTCCTAG-3' |
| VDAC1 alanine mutation | 5'-GCCGATCTTGGCGCGTCCGCCGCGGATGTCTTCACCGCGGGCTACGGCTTTG-3' | 5'-CAAAGCCGTAGCCCGCGGTGAAGACATCCGCGGCGGACGCGCCAAGATCGGC-3' |

**B. Primers sequence of RT-qPCR for mRNA expression**

| Gene Name | Forward Primer | Reverse Primer |
|---|---|---|
| *Cxcl10* | 5'-CCAAGTGCTGCCGTCATTTTC-3' | 5'-GGCTCGCAGGGATGATTTCAA-3' |
| *Endog* | 5'-ACCAGAATGCCTGGAACAAC-3' | 5'-ATCAGCACCTTGAAGAAGTGT-3' |
| *Gapdh* | 5'-GACTTCAACAGCAACTCCCAC-3' | 5'-TCCACCACCCTGTTGCTGTA-3' |
| *Ifi44* | 5'-CTGATTACAAAAGAAGACATGACAGAC-3' | 5'-AGGCAAAACCAAAGACTCCA-3' |
| *Ifit1* | 5'-CAAGGCAGGTTTCTGAGGAG-3' | 5'-GACCTGGTCACCATCAGCAT-3' |
| *Ifit3* | 5'-TTCCCAGCAGCACAGAAAC-3' | 5'-AAATTCCAGGTGAAATGGCA-3' |
| *Ifna4* | 5'-CTTTCCTCATGATCCTGGTAATGAT-3' | 5'-AATCCAAAATCCTTCCTGTCCTTC-3' |
| *Ifnb* | 5'-CCCTATGGAGATGACGGAGA-3' | 5'-CCCAGTGCTGGAGAAATTGT-3' |
| *Iigp1* | 5'-CTATGACTTCCCCGTCCTGA-3' | 5'-TCAGAAATTGCCGCTTCTTT-3' |
| *Isg15* | 5'-CTAGAGCTAGAGCCTGCAG-3' | 5'-AGTTAGTCACGGACACCAG-3' |
| *Oasl2* | 5'-GGATGCCTGGGAGAGAATCG-3' | 5'-TCGCCTGCTCTTCGAAACTG-3' |
| *Rsad2* | 5'-ACACAGCCAAGACATCCTTC-3' | 5'-CAAGTATTCACCCCTGTCCTG-3' |
| *Usp18* | 5'-GAGAGGACCATGAAGAGGA-3' | 5'-TAAACCAACCAGACCATGAG-3' |
| *Vdac1* | 5'-ACTAATGTGAATGACGGGACA-3' | 5'-GCATTGACGTTCTTGCCAT-3' |

**C. Primers sequence of qPCR**

| Name | Forward Primer | Reverse Primer |
|---|---|---|
| D-loop1 | 5'-AATCTACCATCCTCCGTGAAACC-3' | 5'-TCAGTTTAGCTACCCCCAAGTTTAA-3' |
| D-loop2 | 5'-CCCTTCCCCATTTGGTCT-3' | 5'-TGGTTTCACGGAGGATGG-3' |
| D-loop3 | 5'-TCCTCCGTGAAACCAACAA-3' | 5'-AGCGAGAAGAGGGGCATT-3' |
| mt-*16s* | 5'-CACTGCCTGCCCAGTGA-3' | 5'-ATACCGCGGCCGTTAAA-3' |
| mt-*Nd4* | 5'-AACGGATCCACAGCCGTA-3' | 5'-AGTCCTCGGGCCATGATT-3' |

**D. Oligos sequence for mtDNA amplification**

| Name | Forward Primer | Reverse Primer |
|---|---|---|
| mtDNA 47 bp | 5'-TCCTCCGTGAAACCAACAACCCGCCCACCAATGCCCCTCTTCTCGCT-3' | 5'-AGCGAGAAGAGGGGCATTGGTGGGCGGGTTGTTGGTTTCACGGAGGA-3' |
| mtDNA 120 bp | 5'-TCCTCCGTGAAACCAACAACCCGCCCACCAATGCCCCTCTTCTCGCTCCGGGCCCATTAAACTTGGGGGTAGCTAAACTGAAACTTTATCAGACATCTGGTTCTTACTTCAGGGCCATCA-3' | 5'-TGATGGCCCTGAAGTAAGAACCAGATGTCTGATAAAGTTTCAGTTTAGCTACCCCCAAGTTTAATGGGCCCGGAGCGAGAAGAGGGGCATTGGTGGGCGGGTTGTTGGTTTCACGGAGGA-3' |

553

554 **Table. S1. Primers and oligos sequence used in this study**. (**A**) Primers sequence for alanine

555 mutation of the VDAC1 N-terminal domain. (**B**) Primers sequence used in RT-qPCR for mRNA

556 expression. (**C**) Primers sequence for qPCR. (**D**) Oligos sequence for mtDNA amplification.

557 **References and Notes**


558 1. M. R. Wieckowski, C. Giorgi, M. Lebiedzinska, J. Duszynski, P. Pinton, Isolation of
559 mitochondria-associated membranes and mitochondria from animal tissues and cells.
560 *Nat Protoc* **4**, 1582-1590 (2009).

561 2. K. Wang *et al.*, A Herpes Simplex Virus 2 (HSV-2) gD Mutant Impaired for Neural Tropism
562 Is Superior to an HSV-2 gD Subunit Vaccine To Protect Animals from Challenge with HSV-
563 2. *J Virol* **90**, 562-574 (2016).

564 3. N. Keinan, H. Pahima, D. Ben-Hail, V. Shoshan-Barmatz, The role of calcium in VDAC1
565 oligomerization and mitochondria-mediated apoptosis. *Biochim Biophys Acta* **1833**,
566 1745-1754 (2013).

567 4. D. Ben-Hail, V. Shoshan-Barmatz, Reconstitution of purified VDAC1 into a lipid bilayer
568 and recording of channel conductance. *Cold Spring Harb Protoc* **2014**, 100-105 (2014).

569 5. C. J. Wienken, P. Baaske, U. Rothbauer, D. Braun, S. Duhr, Protein-binding assays in
570 biological liquids using microscale thermophoresis. *Nat Commun* **1**, 100 (2010).

571 6. M. C. Hochberg, Updating the American College of Rheumatology revised criteria for the
572 classification of systemic lupus erythematosus. *Arthritis Rheum* **40**, 1725 (1997).

573 7. D. D. Gladman, D. Ibanez, M. B. Urowitz, Systemic lupus erythematosus disease activity
574 index 2000. *J Rheumatol* **29**, 288-291 (2002).

575 8. M. F. Denny *et al.*, A distinct subset of proinflammatory neutrophils isolated from
576 patients with systemic lupus erythematosus induces vascular damage and synthesizes
577 type I IFNs. *J Immunol* **184**, 3284-3297 (2010).

578 9. C. Lood *et al.*, Neutrophil extracellular traps enriched in oxidized mitochondrial DNA are
579 interferogenic and contribute to lupus-like disease. *Nat Med* **22**, 146-153 (2016).
580 10. D. Ben-Hail *et al.*, Novel Compounds Targeting the Mitochondrial Protein VDAC1 Inhibit
581 Apoptosis and Protect against Mitochondrial Dysfunction. *J Biol Chem* **291**, 24986-25003
582 (2016).
583